Tellus (1998), 50B, 521–542
Printed in UK – all rights reserved

TELLUS
ISSN 0280–6509

Aerosol and pollutant transport and their impact on radiative forcing over the tropical Indian Ocean during the January–February 1996 pre-INDOEX cruise

By T. N. KRISHNAMURTI[1]*, B. JHA[1], J. PROSPERO[2], A. JAYARAMAN[3] and V. RAMANATHAN[4],
[1]*Department of Meteorology, Florida State University, Tallahassee, FL32306, USA;* [2]*University of Miami, Miami, FL33149, USA;* [3]*Physical Research Laboratory, Ahmedabad-380009, India;* [4]*Scripps Institute of Oceanography, UCSD, La Jolla, CA, USA*

(Manuscript received 16 October 1997; in final form 12 August 1998)

ABSTRACT

Measurements of aerosol bulk composition, optical depth, size distribution and the incoming solar radiation flux were carried out over the coastal waters of India, the Arabian sea and the tropical Indian Ocean during a cruise conducted in January 1996. Aerosol concentrations were relatively high throughout much of the cruise, even when the ship was at considerable distances from land. In this paper, we link the observed spatial variations and meridional gradients in the measurements to monsoonal and inter-hemispheric transport across the ITCZ using a high resolution global reanalysis that highlights the winter monsoon. We show that the northeast monsoonal low level flow can transport sulfates, mineral dust and other aerosols from the Indian sub-continent to the ITCZ within 6 to 7 days. These transports result in an increase the aerosol optical depth (AOD) at the equator by as much as 0.2 and a decrease in the solar radiative forcing at the sea surface by about 10 to 20 Wm^{-2}. The high concentrations of continental aerosols are a result of three factors: strong (about 6 to 10 m/s) near-surface northerly flow; a shallow boundary layer of about 400 to 800 m thick, which traps the pollutants; subsidence, associated with the northeast monsoon, which suppresses rainfall over most of the Arabian sea and thus minimizes the wet removal process. In addition dust can be transported in the middle troposphere from the Arabian desert to the cruise region 4000 km away with a transit time of 2–3 days. There is strong evidence of interhemispheric transports effected by eddies that wrap around the ITCZ. These eddies bring clean southern hemisphere air to about 10° N in the Indian Ocean and carry polluted continental air into the southern-hemisphere. In this manner, substantial amounts of aerosols and other pollutants can be routinely transported to the southern-hemisphere Indian Ocean during the northeast monsoon. Thus, in order to understand the connection between continental emissions and impacts over the Indian Ocean, it is necessary to focus on the rôle of the northeast monsoon in the large-scale atmospheric circulation over this region.

1. Introduction

One of the largest sources of uncertainty in validating model predictions of climate change is the rôle of aerosols in the radiation budget (IPCC, 1995). Due to their short residence times, aerosols are not uniformly mixed around the globe; consequently, their chemical and physical characteristics, including radiative properties, are subject to substantial regional variations. This variability makes it difficult to assess aerosol radiative forcing on a global scale (Kiehl and Briegleb, 1994). The transport of aerosols from source regions on the

* Corresponding author.
email: tnk@io.met.fsu.edu

continents to the remote oceans could play a significant rôle in the global radiative forcing. The primary objective of this study is to understand the extent to which continental aerosols, both natural and anthropogenic, can be transported over clean ocean areas hundreds and thousands of kilometers away from sources and to characterize the meteorological processes responsible for this transport.

The focus of the study is the Arabian Sea which is surrounded by arid and semi-arid regions which are a source of wind-blown dust particles as well as anthropogenically-produced sulfate and carbonaceous particles. We know very little about the transport of these aerosols or their effects on radiative forcing over the Arabian Sea and the larger Indian Ocean. The ideal time to examine this aspect of the aerosol-climate problem is during the winter monsoon when the prevailing low-level winds are north-easterly, blowing from the Indian sub-continent towards the Arabian Sea and the tropical Indian Ocean. Thus conditions are ideal during winter for the study of the transport of continental materials over the ocean surface, the formation of new particles during transit and the consequent radiative forcing of the aerosol products.

Our study is based on aerosol and radiation data collected from a research vessel on a cruise in the Arabian Sea and the tropical Indian Ocean. For characterizing transports, we used meteorological fields obtained through a high resolution reanalysis described in Krishnamurti et al. (1991). The unique aspects of this reanalysis are twofold: (i) it is based on a physical initialization which is critical for the tropical monsoonal flows; (ii) the reanalyzed fields are computed on a horizontal grid of 70 km $\times$ 70 km. Such high resolution is necessary for distinguishing small-scale features such coastal flows and the structure of the ITCZ, all of which are fundamental for assessing aerosol transport.

The cruise was a preliminary component of a comprehensive international field campaign, the Indian Ocean Experiment (INDOEX) (Ramanathan et al., 1995, 1996) which will take place in early 1999 with the objective of studying the aerosol-chemical-microphysical-radiative interactions over the southern Arabian Sea and the equatorial Indian Ocean. A series of pre-INDOEX cruises on ships-of-opportunity are being conducted before the main field phase. The first of these was on the R/V Malcom Baldrige (Rhoads et al., 1998) in March–April 1995; the protocol included vertical profiles of ozone and water vapor, and extensive measurements of aerosols and gases. There were very large temporal and spatial variations in all properties which could be associated with changes in air-mass characteristics; air masses from the Arabian Sea showed dramatically higher concentrations of aerosol and gas species that are typically associated with polluted continental sources (Rhoads et al., 1998).

Our present study focuses on the second pre-INDOEX cruise which was conducted during 5 January–4 February 1996 aboard the Indian research vessel ORV Sagar Kanya during which research groups from India and USA participated. Measurements included aerosol mass concentration, size distribution, and the concentration of trace gases. In addition there was a very extensive series of radiation measurements, including AOD and spectral-to-broad-band solar fluxes at the sea surface. Jayaraman et al. (1998) describe the results of the aerosol measurements and direct radiative forcing. In this present paper we attempt to link the oceanic aerosol forcing described in Jayaraman et al. (1998) with additional speciated aerosol concentration data (described herein) and with an analysis of the meteorological processes that control transport from the continents.

2. Experiment

Table 1 gives a list of observations and instruments used in this study including those presented in Jayaraman et al. (1998).

2.1. *Cruise history*

Fig. 1 shows the ship's track. The research vessel left Goa, India, 4 January 1996, sailed in the Arabian Sea and the Indian Ocean down to 5° south and returned to Bombay on 4 February. The cruise took place during the northeast monsoon when clear-to-broken low cloud conditions usually prevail north of about 4° N and when the ITCZ is located at the equator or south of it. Both during the initial and final phases of the cruise, observers aboard the ship reported that the sky was nearly cloud-free north of about 4° N. During

Table 1. *Data from the following observations made in the ORV Sagar Kanya cruise (#109) during 5 January to 4 February 1996 are used in the present study (following Jayraman et al., 1998)*

Parameters measured	Instruments used	Responsibility
(i) bulk aerosol samples of nss-mineral aerosols and others		University of Miami, Miami
(ii) aerosol optical depths at 399, 497, 667, and 1051 nm	Hand-held sun-photometer	Physical Research Laboratory, Ahmedabad, India
(iii) aerosol mass concentration and size distribution (0.025, 0.05, 0.1, 0.2, 0.4, 0.8, 1.6, 3.2, 6.25, 12.5 mm radii)	Quartz Crystal Microbalance (QCM) cascade impactor, California Measurements Inc. USA	Physical Research Laboratory, Ahmedabad, India
(iv) direct solar flux (W/m^2) broad band (280–2800 nm) and NIR (780–2800 nm)	pyrheliometer with filter wheel (normal incidence), Eppley Laboratory Inc., USA	Physical Research Laboratory, Ahmedabad, India
(v) global flux (W/m^2) broad band (280–2800 nm) and NIR (780–2800 nm)	pyranometers (2 nos.) Eppley Laboratory Inc., USA	Center for Clouds, Chemistry and Climate, Scripps Institute of Oceanography, San Diego, USA
(vi) spectral global flux (W/m^2) (305, 320, 380 (10 nm FWHM) and PAR (400–700 nm))	Photodiode Radiometer Biospherical Instruments Inc., USA	Center for Clouds, Chemistry and Climate, Scripps Institute of Oceanography, San Diego, USA

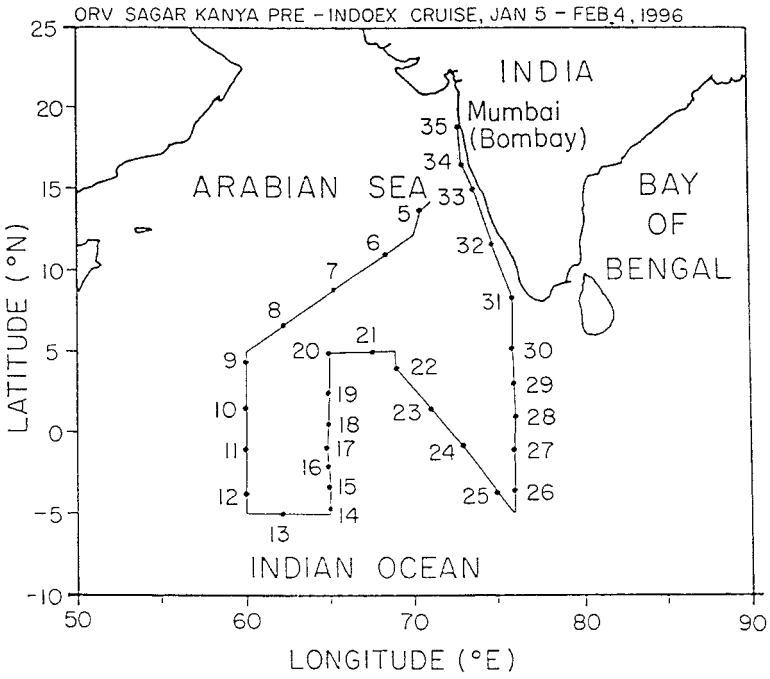

Fig. 1. The track of ORV Sagar Kanya, the Pre-INDOEX cruise made in 5 January to 4 February 1996. The Julian day numbers are marked along the ship track for each day at 12:00 GMT.

the period 20–31 January, however, the sky was cloudy, and deep convective clouds were seen over the equator; thus it was not possible to make radiation measurements during this period. These onboard visual observations are consistent with the sky conditions that we inferred from polar orbiting NOAA satellite data, described next.

2.2. Satellite observations

The cloud cover derived from the AVHRR imagery (shown in Jayaraman et al., 1998) using spatial coherence analyses (Coakley and Baldwin, 1984) indicated that the area-mean cloud cover between the start of the cruise and 8° N ranged between 10 and 25%, with the cloud tops well within the boundary layer. Subsequently, the Sagar Kanya sailed into the ITCZ, south of the equator. In this portion of the cruise the infrared brightness temperatures (IRBT) were below 240 K and the rainfall greater than 8 mm/day. This range of IRBT's is typical of upper-troposphere clouds generated by deep convection. The ship sailed north out of the ITCZ into relatively undisturbed conditions and then returned to the ITCZ during the later phase of the cruise. At the end of the final leg, the Sagar Kanya reentered a region of predominantly clear skies off the western coast of India.

2.3. Aerosol sampling procedures

Daily bulk concentrations were measured by drawing air through Whatman-41 filters (20×25 cm) at a flow rate of about 0.8 m^3/min. To minimize contamination from the ship itself, the sampler was placed above the bridge, well forward on the ship, and the pump was electronically controlled so that it was activated only when the winds came from a 270° sector centered on the bow and when the velocity exceeded 2 m/s. Filters were changed once a day in the morning. A procedural blank filter sample was taken for every 4 exposed filters by manipulating an unexposed filter through the sampling protocol without actually drawing air through it. In the marine boundary layer (MBL), the aerosol collection efficiency of Whatman-41 filters is essentially 100% for nss $SO_4^=$ (Pszenny et al., 1993) and greater than 95% for NO_3^- and 99% for mineral dust (Savoie, 1984).

The exposed bulk filters were individually sealed in plastic bags and returned to Miami for chemical analysis. In Miami, a quarter of each bulk filter was extracted with 20 ml of 18 MΩ cm Milli-Q water in three separate aliquots of 10, 5 and 5 ml. Sample solutions were measured for Na^+ with a standard deviation of $\pm 2\%$ by flame atomic absorption and Cl^-, NO_3^-, $SO_4^=$ and methanesulfonate acid (MSA) within $\pm 5\%$ by suppressed ion chromatography (Savoie et al., 1989a) and NH_4^+ within 10% by automated colorimeter. Non sea-salt (nss $SO_4^=$) is calculated as total $SO_4^=$ minus Na^+ concentration times 0.2517 (i.e., the $SO_4^=/Na^+$ mass ratio in bulk sea water). The bulk filters were also analyzed for mineral dust by ashing the extracted filters at 500 °C for several hours and weighing the residue. During the extraction process, some soil components (e.g., gypsum) are dissolved and, during the heating process, volatile materials (e.g., bound water, halides, carbonates) in the dust can be vaporized; to correct for these losses, we derived the dust concentration from the ash weights by multiplying with a factor of 1.3. This factor was empirically determined after plotting the normal losses. This factor could have an error of $\pm 30\%$. Further work is needed in this area.

Because the filters collect HNO_3 vapor with high efficiency, we consider our measured NO_3^- concentrations to represent total inorganic NO_3^-, that is, aerosol plus gaseous HNO_3 (Savoie et al., 1989a). However, the concentration of gaseous HNO_3 in the near-surface MBL is typically around 20% or less of the total NO_3^- (Savoie and Prospero, 1982; Pszenny et al., 1993). The concentration of NH_4^+ reported here should be regarded as the total of aerosol NH_4^+ plus any gas-phase NH_3 that might react with un-neutralized acid species on the filter (e.g., nss-$SO_4^=$ and NO_3^-).

2.4. Aerosol microphysical properties

The AOD measurements discussed herein were made using a manually operated hand-held sun-photometer at five wavelength bands selected by interference filters centered at 399 nm, 497 nm, 667 nm, 848 nm and 1051 nm and having bandwidths (full width at half maximum) 19 nm, 13 nm, 13 nm, 14 nm and 25 nm respectively. Measurements were also made with an automated sun-photometer (Space Physics Laboratory, Trivandrum) whose results were consistent with

those used in our study. The filter's transmission characteristics were periodically calibrated in the laboratory using a spectrophotometer; the effective central wavelength of the filters (transmission weighted by photodiode response and the solar spectral intensity) is used to convert the measured radiation intensity into AOD. The photometer is manually aimed at the Sun and the peak voltage is recorded during clear sky conditions and for solar zenith angles up to 70°. The total field of view of the photometer is relatively large, 8°, to facilitate the pointing of the instrument towards the sun from the ship deck.

The total optical depth, is calculated from the measured voltage, V and the air mass factor, $1/\mu$ where $\mu = \cos\Theta$ and Θ is the solar zenith angle at the time of measurement. The instrument constant V_O, the "no atmosphere" condition, is obtained by Langley plots made periodically at Mount Abu, a hill station about 1.7 km above mean sea level in northern India (25° N). The V_O values are corrected for the mean sun-earth distance for the day.

The AOD, δa, is obtained from δ after subtracting the optical depths due to Rayleigh scattering and absorption by ozone and water vapor. Rayleigh scattering is calculated assuming an average air column density value of 2.16×10^{25} molecules/cm^2; the annual variation in the air column density is less than 2% (Sasi and Sengupta, 1986) and is not considered in the present study. Ozone absorption is computed from Dobson ozone measurements made at Ahmedabad (23°00′ N, 72°40′ E) for over 30 years (Angreji, 1989); computed values are 0.01 and 0.017 for the 497 and 667 nm channels (weighted for the entire bandwidth) respectively. No corrections were made for the seasonal variation in the column concentration of ozone, about 4%. Water vapor absorption is computed from a constant model water vapor density value of 17 g/m^2 applicable for the Arabian and Indian Ocean for the months of January and February (Sarkar et al., 1982); computed values are 0.035 and 0.018 for the 667 and 1051 channels respectively. The small NO_2 absorption at 399 and 497 nm is ignored. The cumulative effect of these assumptions in the retrieved AOD is expected to be less than 15% for typical AOD values.

2.5. *Aerosol size distribution*

A quartz crystal microbalance cascade impactor (PC-2, California Measurements Inc., USA) was used for the measurements of mass concentration and the size distribution of particles. The ten-stage impactor operates at a flow rate of 240 ml/min with 50% cut off at 0.025, 0.05, 0.1, 0.2, 0.4, 0.8, 1.6, 3.2, 6.25 and 12.5 μm diameter at ambient temperature and relative humidity (Jayaraman et al., 1998). Aerosol number size distributions were derived from the impactor mass-size data; these could be well fitted by the Junge's power law curve of the form, $dn/d(\log r) = K\gamma^{-v}$, in the radius range 0.1 to 10 μm (Bullrich, 1964). Here K is a constant depending upon the number of particles per cubic centimeter, γ is particle radius and v is the slope of fitted power law curve. Fig. 2 shows a time series from 5 January to 4 February 1996 for daily average aerosol size distributions. A high v value along with a high K is an indication of the presence of an increased number of submicron particles relative to supramicron particles.

2.6. *Radiation measurements*

Direct solar radiation measurements were made using calibrated Eppley normal incidence pyroheliometers. We had two independent estimates for the surface global solar flux for $\lambda < 800$ nm. We deployed a Biospherical Instruments Inc. (San Diego, California) model GUV-531 multichannel solar ultraviolet/visible radiometer system, hereinafter referred to as the "photodiode radiometer." The channel of interest here is the so-called photosynthetically active radiation (PAR) channel, which covers the wavelength range 400–700 nm. Lastly, a pair of Eppley PSP pyranometers were deployed, one for measurements of global solar flux in the 280 to 2800 nm

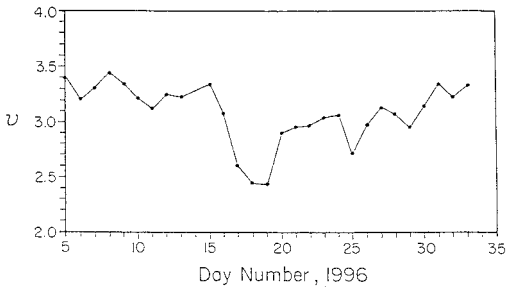

Fig. 2. Time series of the slope v of the Junge power low curve fitted to the daily mean of the measured aerosol size distribution derived from the quartz crystal cascade impactor in the size range 0.1 to 10 μm radius.

and the other in the 780 to 2800 nm wavelength regions. The radiometric instruments was well as the data reduction techniques are described in greater detail in Jayaraman et al. (1998) have an error of $\pm 30\%$.

3. High-resolution global reanalysis

The reanalysis of the meteorological fields used in this study is based on physical analysis procedures developed at FSU (Krishnamurti et al., 1991). Physical initialization was performed using a very high resolution, T-170, global spectral model (space resolution of roughly 70 km at the equator). The observed rainfall used during physical initialization was based on surface and satellite rainfall as described in Gairola and Krishnamurti (1992). The physical initialization involves rainfall and OLR assimilation using several reverse algorithms: (i) a reverse cumulus parameterization; (ii) a reverse surface similarity; (iii) where the model-based outgoing long wave radiation values are relaxed towards satellite-based values.

This process restructures the humidity profiles along the vertical and spins up the convective heating, divergence, and the related fields so as to be consistent with the observed rain rates. The diabatic heating and divergence fields evolve during the physical initialization, consistent with the improved rain rates. The surface fluxes also become well-defined with robust air-sea coupling. Therefore, we feel that our reanalysis is dynamically and thermodynamically much more consistent than the original ECMWF analysis. As an example, the analyzed fields for 7 January 1996 and 2 February 1996 are shown in Figs. 3, 4; these are representative of the upper and lower level streamline field during a very active phase of the winter monsoon. Fig. 3a shows the 1000 mb flow field along with the AVHRR IR radiances in Fig. 3b. The very low values of channel 4 radiances suggest cold and thick upper tropospheric clouds, typical of the ITCZ. Thus, if the analysis is accurate, low-level convergence regions should correspond with low IR radiances.

The strong northerly flows at the 1000 mb over the Arabian sea and Bay of Bengal (Fig. 3a, 4a) are typical of the northeast monsoon. We note a very rapid veering of these flows such that at 850 mb the flows are northeasterlies over the Arabian Sea becoming almost due easterlies over the Bay of Bengal and the south-eastern Arabian Sea. The northerly surface flow (1000 mb) changes abruptly to southwesterlies over the Arabian peninsula. At the 200 mb level, southwesterly flow prevails south of 10° N, veering to westerlies north of 10° N. The implications of the above flow patterns to the aerosol transport are as follows:

(i) The northerly low-level flow from the Arabian Sea into the Indian Ocean can carry pollutants and aerosols from the Indian subcontinent. The low level flow from the Arabian Peninsula, on the other hand, is steered away from the Arabian Sea and thus precludes the transport of Arabian desert dust to the Arabian Sea at this time of year. The southern hemisphere trades carry relatively clean air around the subtropical high located at 30° S and 70° E.

(ii) The deep northerlies seen over the western Arabian Sea and the Bay of Bengal can carry pollutants and aerosols in the boundary layer all the way to the ITCZ.

(iii) The transport patterns can be quite different for pollutants and aerosols that penetrate the boundary layer to the free troposphere. The westerly flow in the mid-to-upper troposphere north of about 10° N can transport mineral dust from the Arabian Peninsula all the way to the Indian sub-continent. Above the boundary layer (about 400 to 800 m thick), the northeasterly-to-easterly flow can carry pollutants all the way to the South African coast between the equator and about 15° S. A difluent asymptote (indicating strong upper tropospheric divergence) is clearly seen in the outflow region of the ITCZ at 200 mb. The minimum speed over the ITCZ and an increase of intensity of the 200 mb wind along the outflowing streamlines is clearly indicative of the strong field of upper tropospheric divergence.

The positions of the low level convergence regions correspond roughly with the cold clouds in the AVHRR image (Figs. 3b, 4b). This agreement gives us confidence in the analyzed fields. In addition, monthly mean rainfall analyses during the cruise are shown in Fig. 5. The distribution and magnitude of rainfall are very similar to the ITCZ location inferred from the AVHRR brightness temperatures shown in Jayaraman et al. (1998). It is important to note an important characteristic of the ITCZ that is revealed by the AVHRR brightness temperatures, the analyzed precipitation field (see the yellow region in Fig. 5)

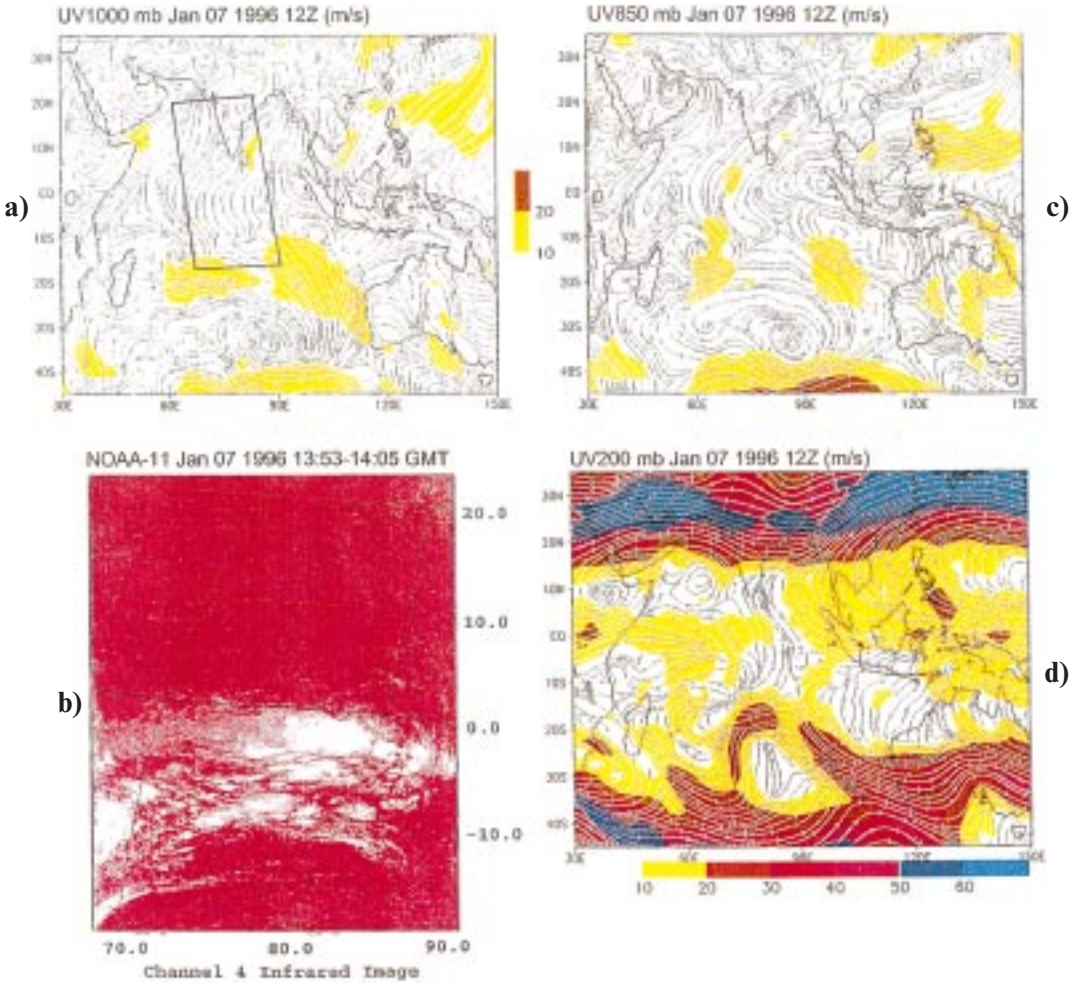

Fig. 3. 24-h streamline and isotach ending on 7 January 1996 at 12 UTC (a) 1000 mb, (b) AVHRR brightness temperature, (c) 850 mb, (d) 200 mb. Units for wind speed:ms^{-1}. Shaded area indicates wind speed according to the scale shown below each figure. Area covered by Fig. 3b is shown by rectangular domain in Fig. 3a.

and the low level flow pattern (Figs. 3a, 4a): it tilts in a south westward direction from about the equator (around 75° E to 90° E) to about 5° S to 15° S (around 40° E to 60° E).

4. Results and discussion

4.1. Bulk aerosol concentration trends

The aerosol concentrations for the principal species (nss-sulfate, nitrate, ammonium and mineral dust, collectively refered to as SNAD) are shown in Fig. 6 plotted along the path of the vessel. The highest concentrations were obtained toward the end of the cruise when the ship was close to the west coast of India. However, relatively high concentrations were observed during most of the cruise, even when the ship was near the equator, at a considerable distance from India and other land masses. Indeed, almost all samples collected during the cruise yielded concentrations of NO_3^- and nss $SO_4^=$ that are substantially greater than oceanic "background" values, about 0.1 μg/m^3 for NO_3^- and 0.3–0.7 μg/m^3 for nss $SO_4^=$ (Savoie et al., 1989b).

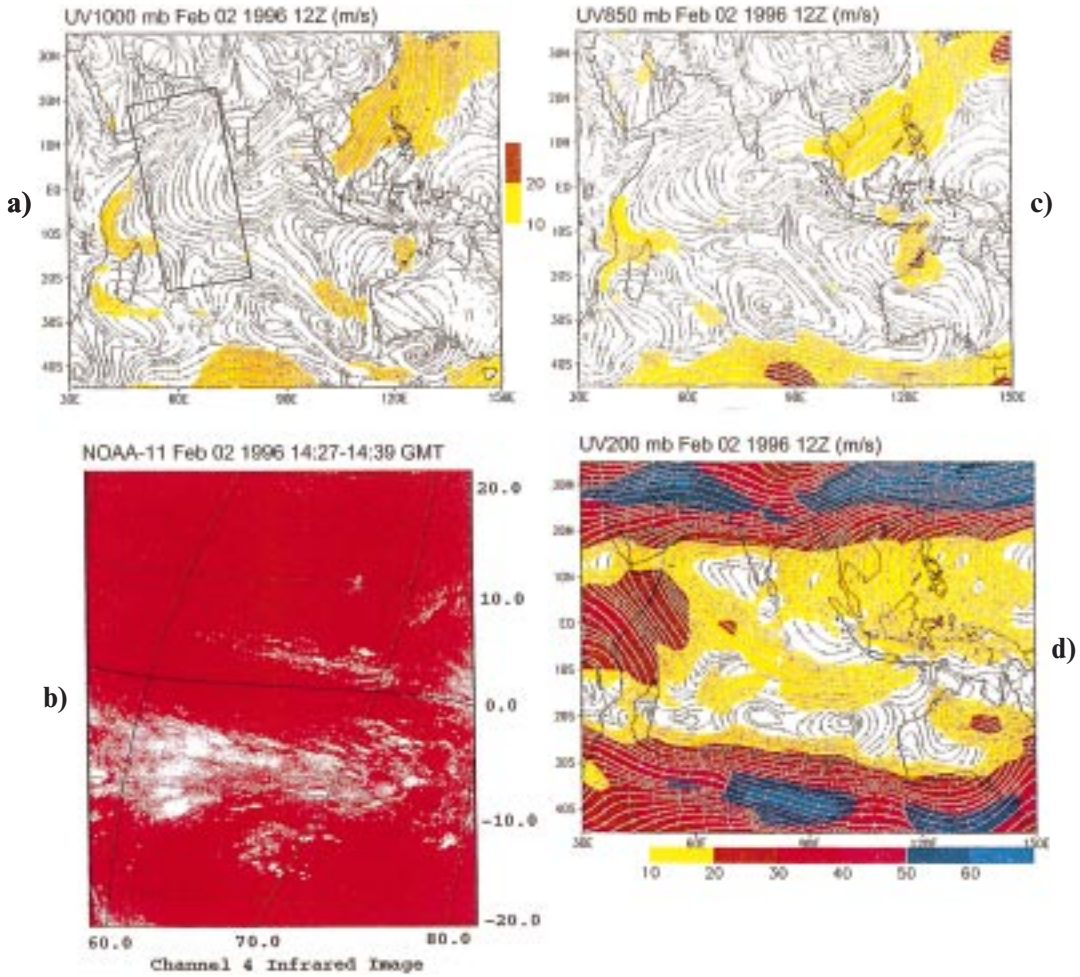

Fig. 4. 24-h streamline and isotach ending on 2 February 1996 at 12 UTC (a) 1000 mb, (b) AVHRR brightness temperature, (c) 850 mb, (d) 200 mb. Units for wind speed:ms^{-1}. Shaded area indicates wind speed according to the scale shown below each figure. Area covered by Fig. 4b is shown by rectangular domain in Fig. 4a.

Our data suggest that the aerosol concentrations are largely driven by transport from continental sources. The contribution of $SO_4^=$ from the oxidation of ocean-derived dimethylsulfide (DMS) is believed to be very small based on the very low concentrations of aerosol methanesulfonate (MSA) that we measured. Fig. 7 shows the concentration of MSA along with that of nss $SO_4^=$. Using MSA, we can estimate the quantity of $SO_4^=$ derived from the DMS. Previous studies have shown that in the low and mid-latitudes of remote ocean regions, the ratio of nss $SO_4^=$ to MSA is relatively constant, about 12–15 (Savoie et al., 1994). Using this ratio, we convert the MSA values into an equivalent concentration of $SO_4^=$ as shown in Fig. 7. It is clear that the oceanic component of $SO_4^=$ is a very minor fraction of the total concentration; only in one case (sample JD 18) did ocean-derived nss $SO_4^=$ constitute a substantial fraction of the total.

The relative concentrations of NO_3^-, nss $SO_4^=$ and NH_4^+ did not vary much throughout the cruise except for the portions close to the coast of India on the return leg (JD 31, 32, 33). The ratios of NO_3^- to nss $SO_4^=$ (Fig. 8a) and NH_4^+ to the sum of nss $SO_4^=$ and NO_3^- (Fig. 8b) fall into two

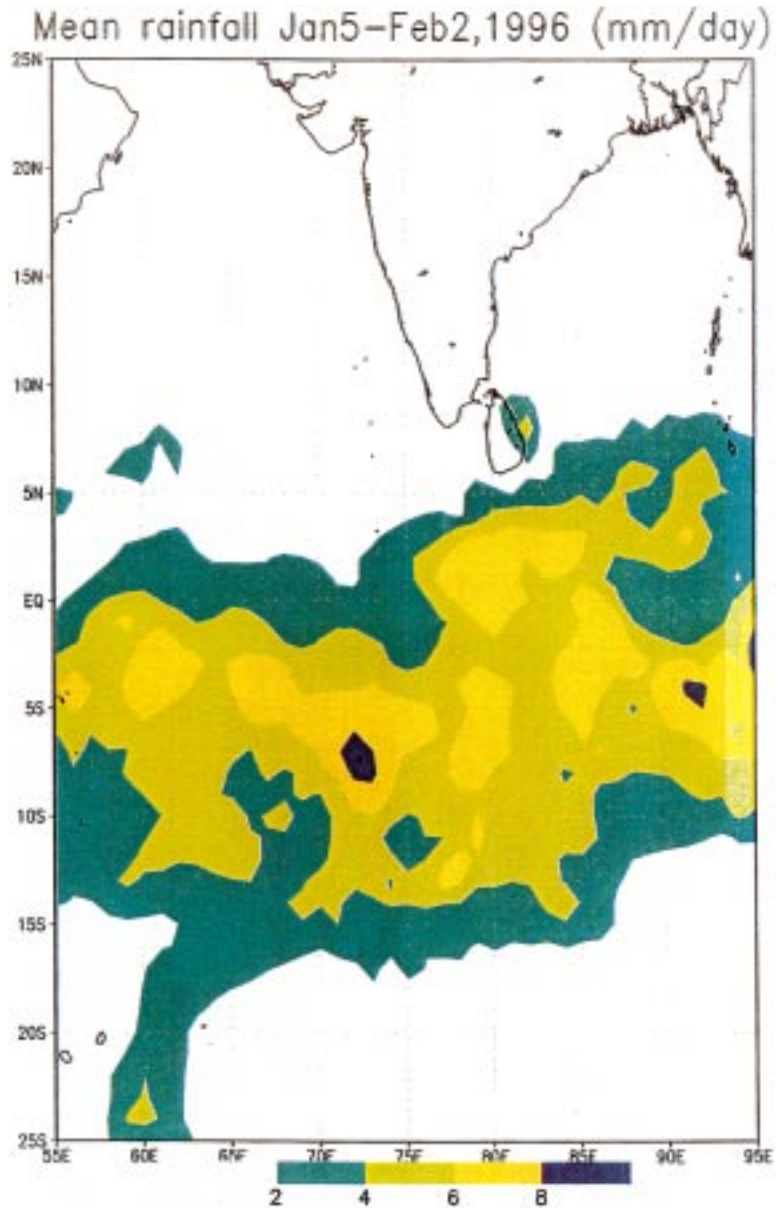

Fig. 5. Monthly mean rainfall for the Pre-INDOEX cruise made in 5 January to 4 February 1996. Units: mm/day. Rainfall amounts over shaded area are according to the scale shown below each.

groups, with the samples for JD 31, 32, and 33 standing out from the remainder of the group, a factor that is emphasized in Fig. 8c, which shows the ratio of nss-$SO_4^=$ to dust. The composition of the samples from JD 31–33 are dominated by mineral dust which comprises about half of the total measured species mass in the samples, including sea salt aerosol. The NO_3^- concentration in samples JD 31–33 is also unusually high as reflected in the ratio of NO_3^- to nss-$SO_4^=$ (expressed in equivalents); it is about 0.3 except for JD 31–33 where it is over 2× as great. Based

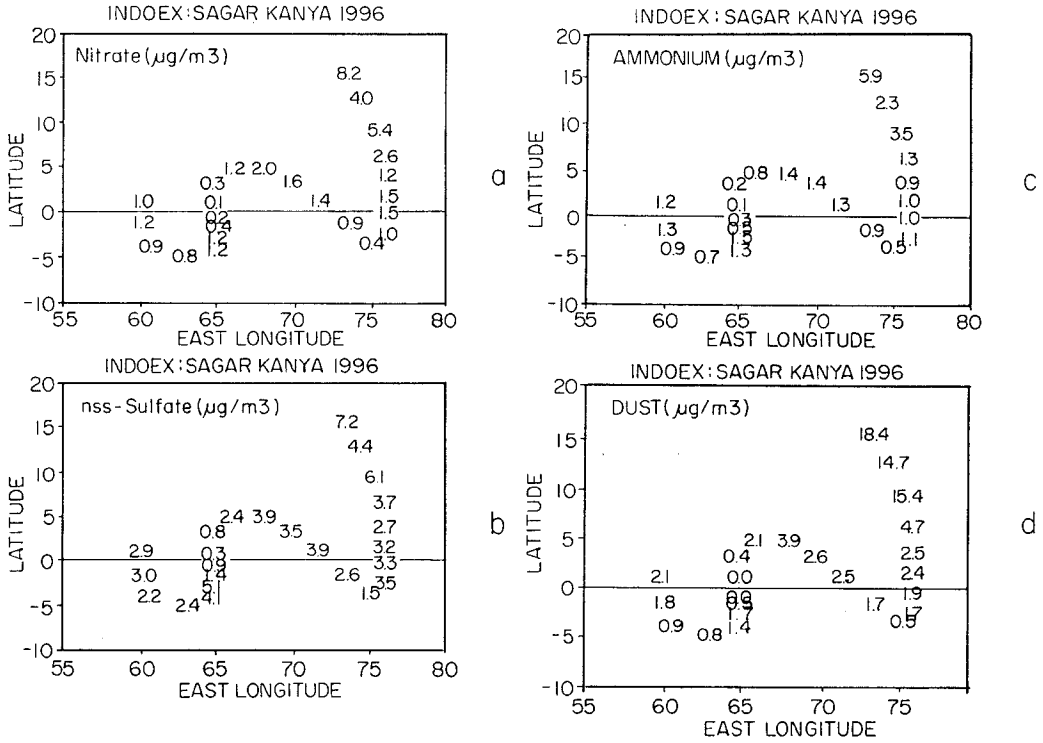

Fig. 6. Daily mean aerosol concentrations during the cruise of ORV Sagar Kanya. Concentrations are plotted at the mid-point of the cruise track during which the sample was collected. Units are μg/m^3. From top to bottom: (a) nitrate; (b) nss-sulfate; (c) ammonium; (d) mineral dust.

on the ratio of NH_4^+ to the sum of the acid species nss-$SO_4^=$ and NO_3^-, the aerosols are somewhat acidic with ratios (measured in equivalents) in the range of 0.6 to 0.8; JD 33, which has a ratio of 1.1, stands out as an exception. However, given that dust is a major constituent in most samples and that neutralizing species such as $CaCO_3$ are common constituents in dust, we might expect that the aerosol samples are considerably less acid than suggested in Fig. 8b.

The mean concentrations measured during the cruise were (in units of μg/m^3): NO_3^-, 1.68, nss-$SO_4^=$, 3.12; MSA, 0.023; dust, 3.52; NH_4^+, 1.31; Na^+, 1.90 (and sea salt, expressed as 3.256*Na, 6.19). The mean aerosol concentration for all species for the entire cruise is 15.84 μg/m^3. These results are consistent with the limited aerosol data that are available for this region. Measurements made during the spring of 1979 during the Global Weather Experiment (Savoie et al., 1987) show that the concentrations of aerosol nss-$SO_4^=$ and NO_3^- are relatively high in the Arabian Sea and northwestern Indian Ocean (nss-$SO_4^=$, 2.7 μg/m^3; NO_3^-, 1.01 μg/m^3); in contrast, in winds from the southern hemisphere, concentrations drop to very low values (nss-$SO_4^=$, 0.50 μg/m^3; NO_3^-, 0.16 μg/m^3). Savoie et al. (1987) attributed the high concentrations of nss-$SO_4^=$ and NO_3^- north of the ITCZ to the transport of pollutants out of India and the Middle East and possibly Europe. Savoie et al. (1987) also found strong gradients in dust concentrations. In northerly winds, the dust mean was 7.59 μg/m^3; in contrast, southern hemisphere winds yielded an average of 0.27 μg/m^3 (Savoie et al., 1987). Indeed, dust concentrations over the Arabian Sea and the NW Indian Ocean close to Africa are comparable to those measured along the west coast of Africa and the Mediterranean (Savoie et al., 1987; Prodi et al., 1983). More recently, in 1995 during the spring cruise of RV Malcom Baldrige, Rhoads et al. (1998) found that in the southern and central

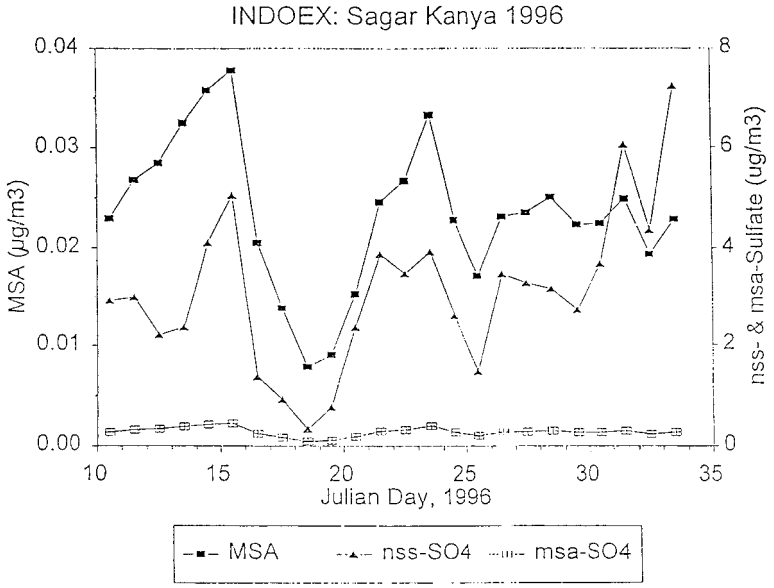

Fig. 7. Time series of the concentration of sulfur species in daily aerosol samples: nss SO_4, methanesulfonate (MSA), and MSA-sulfate (the concentration of sulfate that might have been derived from oceanic dimethylsulfide, calculated on the basis of the concentration of MSA; see text for details).

Indian Ocean south of the ITCZ, NO_3^- aerosol concentrations were typically in the range of 0.1–0.2 µg/m^3; nss-$SO_4^=$ was typically in the range 0.1–0.5 µg/m^3. North of the ITCZ, NO_3^- concentrations were sharply higher, typically ranging from 0.5 to 2 µg/m^3 with values as high as 3.5 µg/m^3; nss-$SO_4^=$ typically ranged from 1 to 4 µg/m^3 with values as high as 9 µg/m^3. Mineral dust concentrations in southern-hemisphere Indian Ocean air masses were below the detection limit (about 0.1 µg/m^3); in contrast, the mean for Arabian Sea air was 6.2 µg/m^3. The concentration distributions and the seasonality observed on these cruises are generally consistent with the aerosol transports shown in AVHRR (Husar et al., 1997), with the absorbing aerosol (dust) transports indicated in Herman et al. (1997) and with the monsoon circulation and the inferred dust distribution (Ackerman and Cox, 1982, 1989).

4.2. *Trends in aerosol size distribution and radiation*

Concurrent complementary aerosol and radiation measurements were made on the same cruise as reported by Jayaraman *et al.* (1998). These are briefly summarized here.

The AOD in the visible wavelength region was in the range of 0.2 to 0.5 over the Arabian Sea and 0.1 and below over the equatorial Indian Ocean. Total aerosol mass concentrations decreased from a high of about 80 µg/m^3 near the coast to very low values of only a few tenths of µg/m^3 over the more distant ocean regions; similarly, the sub micron size (<0.1 µm) particles showed more than an order of magnitude decrease in the number concentration. The large increase in the small particle concentrations near the coast was also consistent with the corresponding large increase in the Angstrom exponent, α, which increased from 0.2 over the Indian Ocean to about 1.4 near the coast.

The radiative forcing from the aerosol was obtained for the direct solar flux and for the global (direct + diffuse) solar flux separately in the UV, visible and near IR spectral regions. The regression of AOD against the flux measurements shows that for an increase of 0.1 in AOD the direct visible (<780 nm) solar flux decreases by about 42 Wm^{-2} and the global flux in the visible region decreases

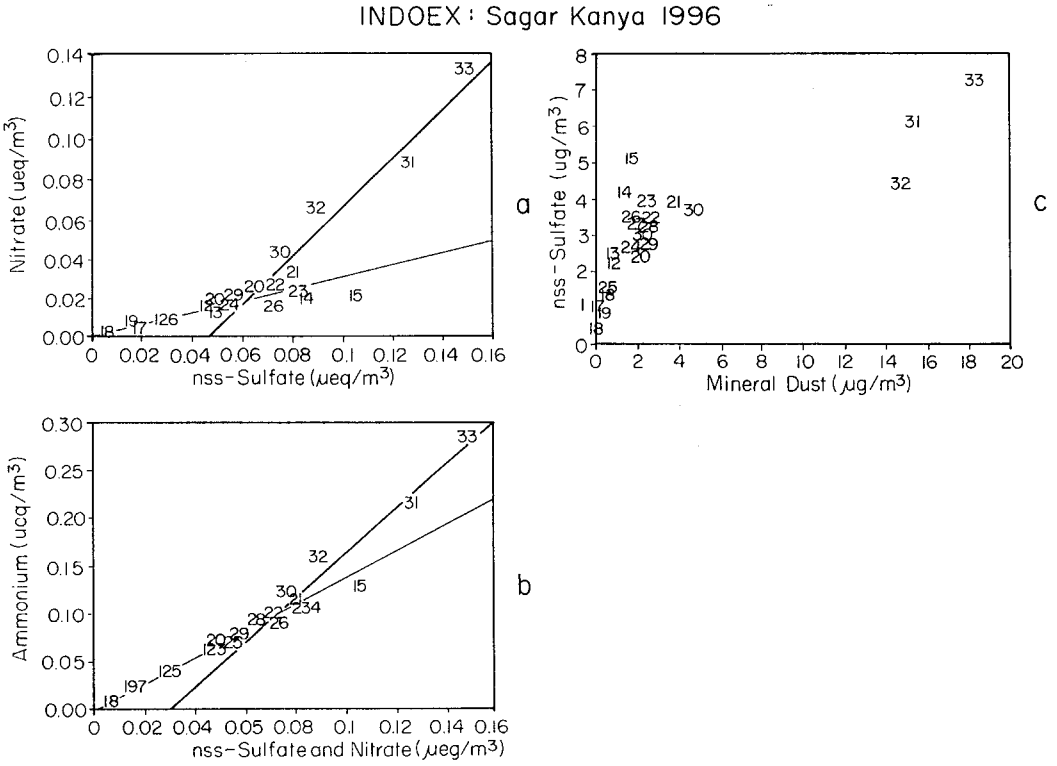

Fig. 8. Scatter plots of aerosol species concentrations. (a) NO_3^- versus nss $SO_4^=$ (microequivalents m^3); (b) NH_4^+ versus the sum of nss $SO_4^=$ and NO_3^-, (microequivalents m^3; (c) nss $SO_4^=$ versus mineral dust. Lines indicate the general strend of relationships of the plotted variables; slopes are marked.

about $14\,Wm^{-2}$ (with an uncertainty of $10\,Wm^{-2}$). For the same extinction AOD, the radiative forcing (direct + diffuse) of the coastal aerosols is larger than the open-ocean aerosol forcing by a factor of 2 or larger. In summary, the data presented here and by Jayaraman et al. (1998) reveal a strong latitudinal gradient in the aerosol mass, number concentration, AOD and radiative forcing, all of which decrease from the Arabian Sea to the equatorial Indian Ocean.

4.3. Relationship of aerosol properties to AOD

In this section, we examine in detail the speciated aerosol chemistry measurements presented in Subsection 4.1 with AOD data (Fig. 9). Nss-Sulfate is derived from biogenic (oceanic) and anthropogenic sources (Hameed and Dignon, 1992). Ammonium is derived primarily form continental sources with some contribution from the oceans. Nitrates are from anthropogenic sources as well as from lightning; the latter might be especially important in the ITCZ region. It should be noted that AOD data are available for only a few days, primarily because of cloud interference. The following are the important features.

(i) Peak AODs (>0.2) were found close to the coast (5, 6 January, 2, 3 February). The high coastal AOD values were accompanied by relatively higher concentrations of small particles (<0.1μm) and relatively high aerosol mass concentrations (>40 μg/m^3 as shown in Jayaraman et al. (1998).

(ii) There is an excellent coherence between variations in AOD and bulk chemical composition. High AODs close to the coast are accompanied by high concentrations (>3 μg/m^3) of SNAD

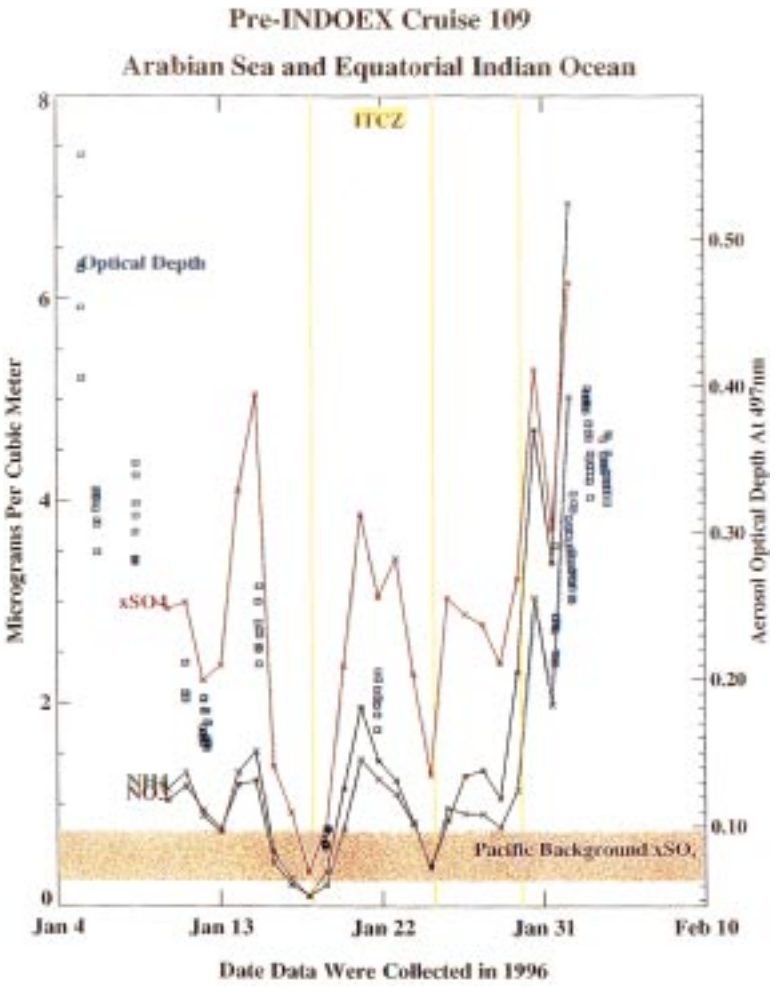

Fig. 9. Time series aerosol mass concentration for $SO_4^=$, NH_4^+, NO_3^-, and aerosol optical depth during the cruise of ORV Sagar Kanya.

from 2–4 February. The lowest AOD on 19 January coincides with very low values of SNAD. In the same way, the AOD decrease from 11–12 January, the increase from 12–15 January, the decrease from 15–19 January and the increase from 19–22 January are all accompanied by similar trends in the concentrations of SNAD.

(iii) The Junge exponent, v, obtained from the daily mean aerosol size distribution shows variations (Fig. 2) similar to that shown for aerosol mass concentrations. In particular, the maxima seen on 15, 21, 26, 31 January and 2 February as well as the minima seen on 18, 25 and 29 January in the SNAD values could be correlated with the maxima and minima in the v values obtained on the same dates. The episodic increases in aerosol concentration and in v observed over the Indian Ocean are attributed to the arrival of air masses carrying "fresh" continental pollutants that are characterized by relatively high concentrations of sub-micron particles.

In this study, we have not considered the contribution of black carbon and organic aerosol as no measurements were made of these species during the cruise period.

4.4. Rôle of transport

Two aspects of computation are noted first.

(a) A three dimensional semi-Langrangian advective algorithm (Krishnamurti et al., 1996) makes use of the analyzed 3-dimensional winds at 6-hourly intervals. These are interpolated to 15-min time-steps and three-dimensional trajectories are constructed.

(b) The cumulus parameterization scheme provides the grid-scale vertical motion (upward and downward); implicitly it also provides cumulus-scale updraft and downdraft mass fluxes and information on the fractional areas of these updrafts and drowndrafts. When this procedure is used to construct trajectories we see that air parcels originating in the lower troposphere often exhibit a very strong ascent in the deep convective areas and they subsequently exit in the upper troposphere.

We compute 7-day back trajectories initiated from the ship position. In Fig. 10 we illustrate the trajectories originating from 990, 900 and 850 mb for the cruise dates of 12, 15, 19, 22 January and 2 February 1996. We focus primarily on the lower levels, because the bulk of the aerosol radiative forcing at the surface is expected to take place in the lowest 1 to 2 km. The following criteria were applied in selecting the 5 days shown in the figure: we selected only those days for which data were available for both the AODs and the aerosol sampling and from these we used only those days when the aerosol AOD and the sulfate concentrations reached near-maximum (15, 22 January,

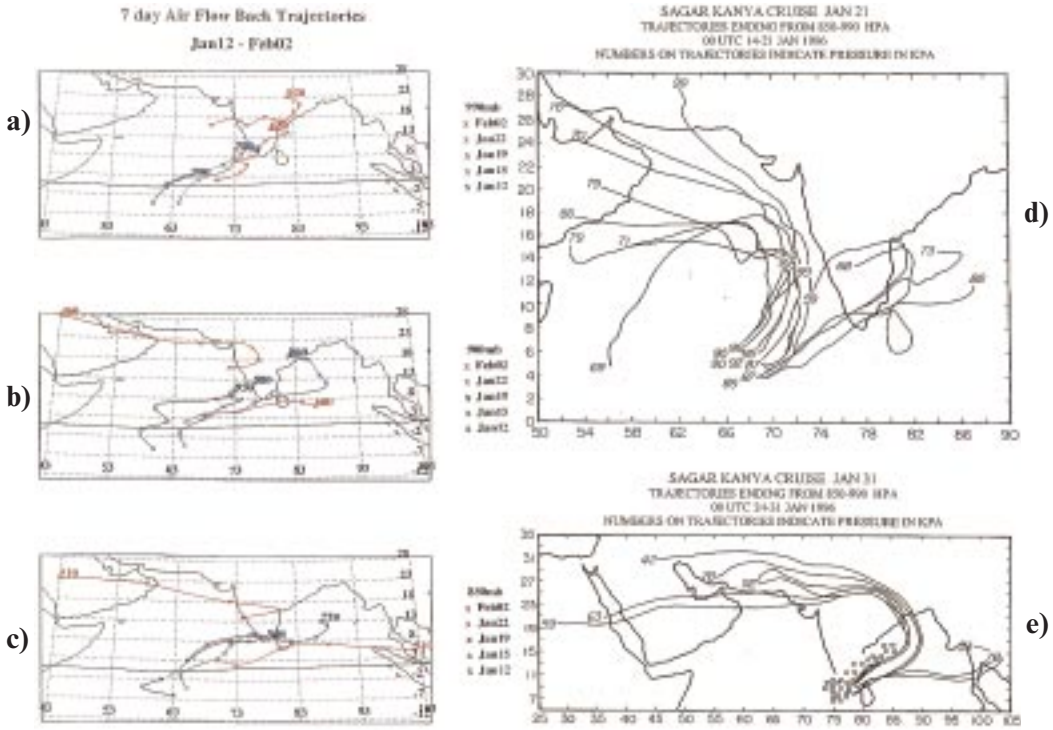

Fig. 10. 7 days back-trajectories for: (a) Starting day 12, 15, 19, 22 January and 2 February; starting level 990 mb. (b) Starting day 12, 15, 19, 22 January and 2 February; starting level 900 mb. (c) Starting day 12, 15, 19, 22 January and 2 February; starting level 850 mb. (d) Starting day 21 January 1996; starting level 990, 975, 950, 925, 900, 875, and 800 mb. (e) Starting day 31 January 1996; starting level 990, 975, 950, 925, 900, 875, and 800 mb. Numbers on trajectories in (a), (b), (c) indicate the pressure at the end of trajectory in hPa; while those in (c), (d) are the starting and ending level pressure in kPa.

2 February) or near-minimum values (12, 18, 25 January).

We see a number of features in these illustrations, Fig. 10a,b,c. Air parcels arrive offshore of the southwest coast of India from the south of the equator and from India at 990 mb. Trajectories indicate Arabian air incursion offshore of southwest India at 900 and 850 mbs. Trajectories overlying the Bay of Bengal also make it offshore of the southwestern India at 900 and 850 mbs. The nature of the computed trajectories suggests that mineral aerosols from the desert region of Arabia as well as from the semi-arid regions of India could make their way into the offshore region of southwest India, see Fig. 10d,e. These two illustrations show a swath of backward trajectories constructed from boundary layer between 990 and 850 mb. A preponderance of Arabian air trajectories do arrive over this region, however some continental air from India must also be conveyed to this region.

Above the boundary layer (900 mb and 850 mb levels), there is a hybrid structure. In the equatorial Indian ocean, the transport is generally from the northeast to southwest. Furthermore, there is transport downwards from a high at 500 mb (see the 22 January trajectory). The picture near the coastal Arabian Sea (2 February) is strikingly different. Air originates from about 400 to 500 mb in Saudi Arabia and descends over the Indian coast, possibly transporting mineral dust. The air travels eastwards and descends, covering about 3000 km in less than 3 days. These are situations of cold outbreaks over northern India, when the northeast monsoon is very shallow; the thermal wind driving these cold outbreaks turns the wind to westerlies (Figs. 3d, 4d). For the most part, the relevant trajectories from northeast India that make it to the Indian ocean (and to the ITCZ) are those that originate in the lowest 1.5 km.

The daily average global (direct + diffuse) solar flux in the 400 to 700 nm region is shown in Fig. 11. The minima in the solar flux occur on 18 and 19 January, which indicates very thick cloud coverage. The surface flow analyses suggests that the clouds on these 2 days over the ship were associated with the ITCZ, i.e., with precipitation systems. To illustrate the fundamental importance of transport in the aerosol radiative-forcing issue, we will consider 4 cases.

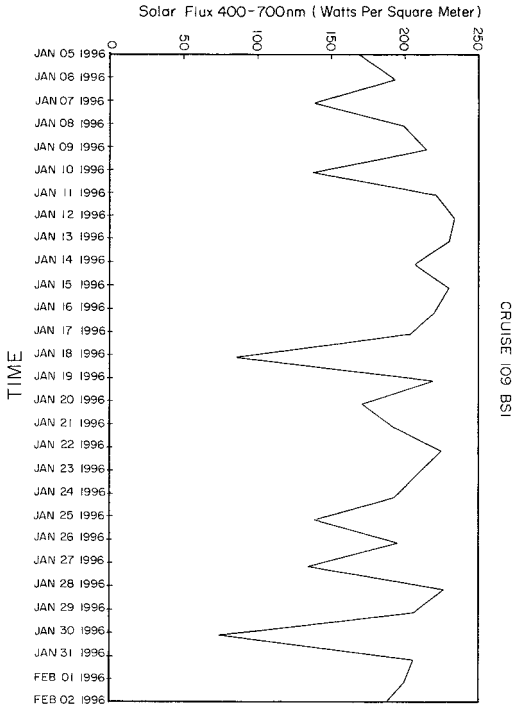

Fig. 11. Time series of daily average global 400–700 nm solar flux as measured aboard ORV Sagar Kanya.

(1) 12, 15 January. The SNAD concentrations and the AODs were relatively low on 12 January and relatively high on 15 January (Fig 9). The ship was at about 5° S on both these days (Fig. 1). The low level (990 mb) back trajectory on 12 January terminates over the ocean, whereas on 15 January the trajectory terminates close to the Indian land mass. Fig. 12 compares the 1000 mb streamline for 12 January with that for 15 January. The strong northerly flow on 15 January as opposed to the almost easterly flow (around 60° E to 75° E near the equator) on 12 January suggests that the increase in SNAD and AOD on 15 January is most likely due to continental sources. Because of the strong low-level northerly flow of about 7 m/s on 15 January, transport from 20° N (central India) to about 5° S can take place in less than 3 days; since there are no precipitating clouds (and, hence, no precipitation removal of aerosols) between 20° N to about 5° S, there are favorable for the long-range transport of continental aerosols. Furthermore, comparison of the mean aerosol size distribution obtained on these

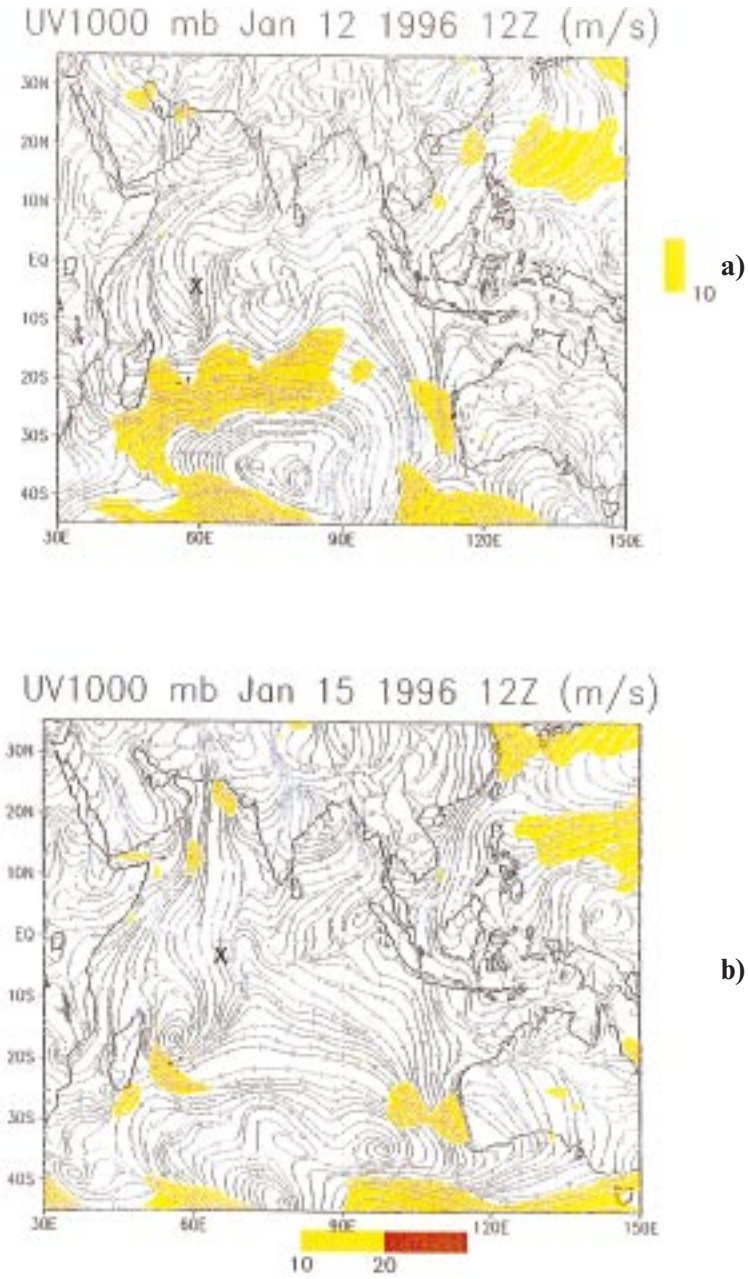

Fig. 12. 24-h streamline and isotach at 1000 mb (a) ending on 12 January 1996 at 12 UTC, (b) ending on 15 January 1996 at 12 UTC. X indicates position of ship on the map date.

two days (Fig. 13a) clearly indicates that there is more than a two-fold increase in the number of sub-micron size particles (0.05 to 0.5 μm radius) on 15 January, supporting our hypothesis that the observed peak in SNAD concentrations on the 15 January is the result of long range transport of particles from the continents.

(2) 18, 22 January. The lowest values of SNAD

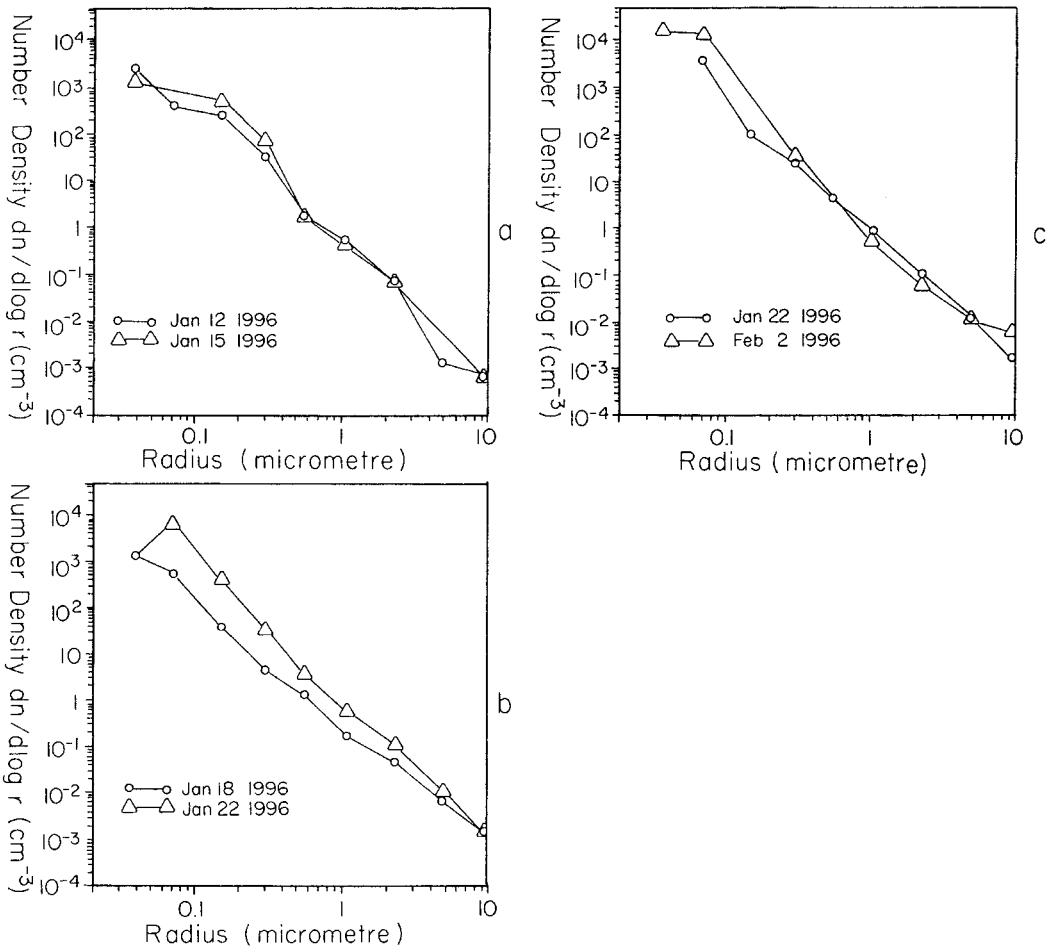

Fig. 13. Aerosol number size distribution calculated from impactor mass distributions assuming a uniform aerosol density of 2 g cm^{-3}. The size distributions in each panel reflect changes associated with a transition from a low concentration day to a high concentration day: (a) 12 to 15 January, (b) 18 to 22 January and (c) 25 January to 2 February.

and AODs were encountered on 18 January when the ship was at about 1° N, 70° E. Further north, on 22 January (5° N, 70° E), sulfate concentration increase almost 8-fold while the AOD increased by a factor of about 2 to 3. Between 17–18 January the ship sailed through a precipitating ITCZ cloud system and, among other changes, the daily averaged solar flux decreased by more than 100 Wm^{-2}. The low level stream flow (Fig. 14) also reveals converging stream lines around the ship location. The lowest aerosol concentrations of the cruise were measured at that time; clearly, wet removal must have been responsible. On 22 January, the ITCZ moved south of 5° S and the flow returned to northerly from the Indian subcontinent (as evidenced by the 990 mb trajectory). This case illustrates some of the fast time scales of the ITCZ migration. Our conclusion about the rôle of wet removal on 18 January is further strengthened by a comparison of the aerosol size distributions on 18 and 22 January (Fig. 13b); on the 18 January, the number concentrations in all size ranges are substantially less than on 22 January. Furthermore, model results reported a rainfall of 0.8 mm on the 18 January.

(3) 25 January. The SNAD concentration at

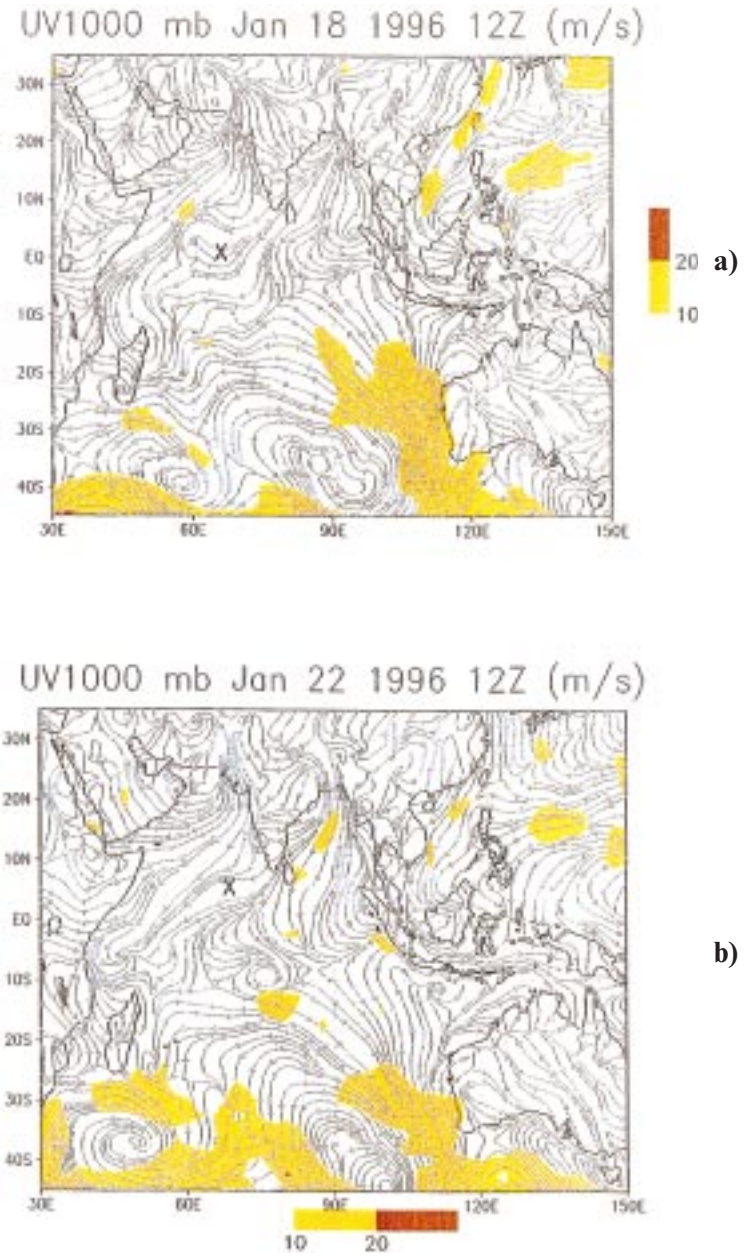

Fig. 14. 24-h streamline and isotach at 1000 mb (a) ending on 18 January 1996 at 12 UTC, (b) ending on 22 January 1996 at 12 UTC. X indicates the position of the ship on map date.

the ship location (4° S, 75° E) returned to very low values again for two reasons. First, the streamline at this location (Fig. 15) originates from 40° S, thus indicating the pristine source of the air mass. In addition, the ship position was sufficiently close to the ITCZ (see the surface solar flux in Fig. 11) that precipitation removal must have played a role.

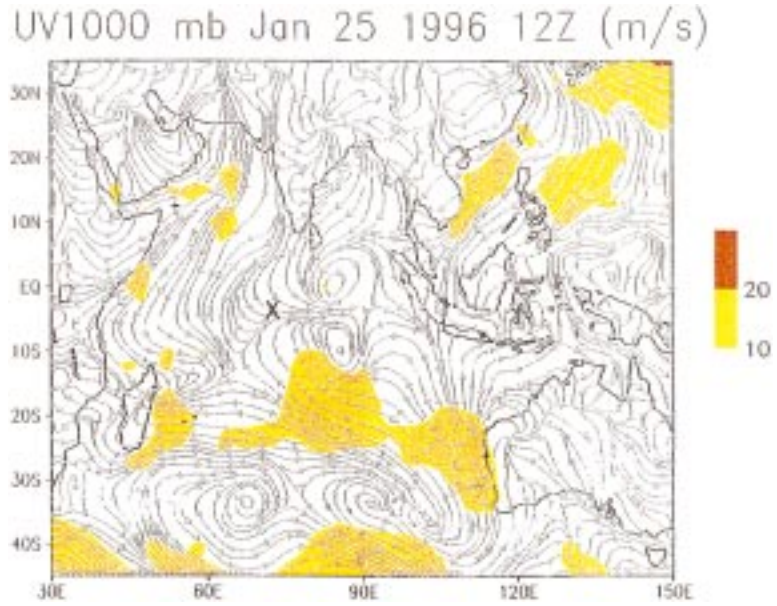

Fig. 15. 24-h streamline and isotach at 1000 mb ending on 25 January 1996 at 12 UTC. X indicates the position of the ship on map date.

2 February. We now focus our attention on the large AOD's observed near the coast. The concentration distribution of dust (Fig. 6) and the time series (Fig. 16) reveals that, close to the coast, the mineral dust increased eightfold. Dust sources in India (e.g., the Rajasthan Desert on the northwestern Indian region) is potentially an important source for the coastal dust. In addition, the 850 mb back trajectory suggests another surprising dust source from the North African deserts; this trajectory originated (5 days ago) from the mid-troposphere of N. African desert (Saudi Arabia and beyond). The relative contribution from local Indian sources and long-range African sources cannot be determined from our data, but will be a subject for future study. The aerosol number density obtained on 2 February (Fig. 13c) shows an increase in the smaller (less than 0.5 μm radius) as well as in the larger (greater than 5 μm radius) size ranges compared to 25 January indicating that the concentration of all particle types (submicron $SO_4^=$, NO_3^- and NH_4^+ and supramicron dust) had increased near the coast.

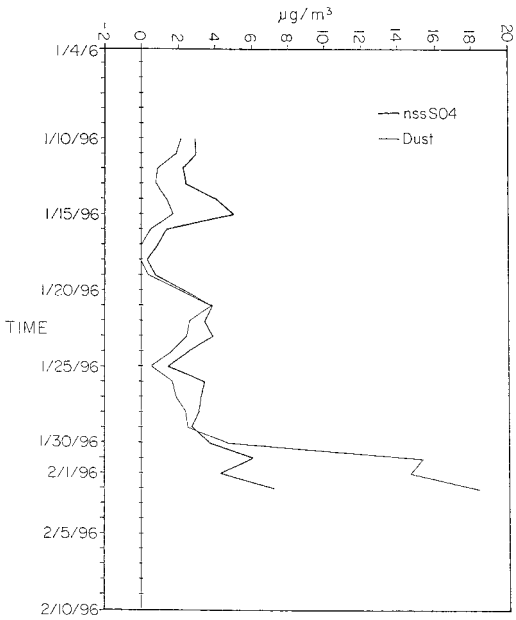

Fig. 16. Time series of surface layer mineral dust and nss-sulfate

4.5. *Rôle of the ITCZ*

The low level convergence zones (and hence the ITCZ) are generally tilted form northwest to sou-

theast direction (e.g., see Fig. 3a, 4a, 12). In other words, in the eastern Indian ocean ($>75^\circ$ E) the ITCZ is closer to the equator, while in the western Indian Ocean ($<65^\circ$ E), it is south of 15° S. As a result, as the ship sailed eastward (from 13 January onwards) it should have encountered more precipitating clouds. This is indeed the case, as can be seen in Fig. 5 (the yellow regions) and also in the AVHRR images (Jayaraman et al., 1998). This northwest-to-southeast tilt has a remarkable impact on transport and aerosol distribution.

East of 80° E, the southern hemisphere air can penetrate as far as 10° N into the Arabian Sea (see, for example, the 25 January stream line, Fig. 15). At the same time, polluted and aerosol-rich air from the northern hemisphere can penetrate as far as 20° S in the western Indian Ocean (Fig. 15).

An important aspect is the fast time scales in which the ITCZ changes direction and intensity. A comparison of the low level convergence zones in Figs. 12, 14 and 15 attests to such changes. Because of the rapid changes in the ITCZ and the steep northwest-southeast slope of the ITCZ, we conclude that during the north-east monsoon period there are significant inter-hemispheric transports taking place in this region. It should perhaps be stated that when the ITCZ is located near 5° S there do exist a large population of convective clouds as far as 5° N. These systems do have vigorous up and down motion, thus facilitating mixing in the vertical. The inter-hemispheric transports over this region do not carry a long fetch of oceanic air transport prior to their crossing of the equator. In this since the winter monsoon is quite different from the oceanic ITCZ of the Pacific and Atlantic Oceans.

4.6. Transport and radiative forcing

Fig. 9 shows that visible AODs can reach as high as 0.2 (12, 18 and 22 January) in the northern and southern hemisphere equatorial ocean (5° N to 5° S). We attribute these high values to strong northerly winds from the Indian sub-continent. The increase was accompanied by an increase in the sulfate concentration to about 1.5 to 5 $\mu g/m^3$ from the background value of about 0.5 $\mu g/m^3$. From Jayaraman et al. (1998) we infer that the instantaneous radiative forcing at the sea surface can decrease by about 20 Wm^{-2} for an AOD of 0.2; diurnally averaged, the value can be as high as 10 Wm^{-2}.

Near the coastal ocean, the AODs increased by about 0.3 to 0.4, while the sulfates increased comparably. The 850 mb back trajectory suggests that part of the increase may be due to transport of mineral dust, as indeed supported by the mineral dust data (Fig. 6 and Fig. 16). According to Jayaraman et al. (1998), the coastal AODs of 0.3 to 0.4 should decrease the diurnally-averaged solar insolation by about 20 to 30 Wm^{-2}.

5. Conclusion

During the northeast monsoon, the aerosol concentrations measured over a large region of the Arabian Sea and the tropical Indian Ocean were much higher than one would expect, especially for the more distant southern hemisphere ocean regions. Meteorological studies show that high aerosol concentrations could be linked to transport from the Indian subcontinent and also from sources in the Middle East and North Africa. Our trajectory studies, especially Fig. 10 d, e, confirms the possibility for the transport of Saharan mineral aerosols over these long distances. Although heavier aerosols may settle down (via dry disposition) these still remain a strong possibility for the lighter aerosols of Arabian (and also possibly from the semi-arid regions of India and Pakistan) to make its way to the region offshore from southern India. The optical depth data sets, presented here, provide a strong case for their possibility.

The variations in aerosol concentration could be linked to the variability of the various radiation measurements that were being made concurrently aboard ship. On this basis we could infer that even relatively modest AOD values (0.2) could result in a decrease in the instantaneous radiative forcing at the sea surface by about 20 Wm^{-2}. Such a large reduction in surface insolation has important climatological implications. Collectively, taking the aerosol and the radiation measurements and the computed four dimensional trajectories we are able to show that: a large gradient of the aerosols is indeed present downwind from the coast of southern India as we enter the Sagar Kanya Cruise area. Between the equator and 4° S we see values of sulfate concentrations as low as

0.5 μg/m^3 to as high values as 3.9 μg/m^3 near the coast around 76° E. This confirms the presence of large concentrations of sulfates quite far away from the source regions and the presence of large gradients near the coast. However, before any firm conclusions can be made, it will be necessary to have a better understanding of the role that these aerosols play in both direct and indirect radiative forcing.

The aerosols are clearly impacted by congenital anthropogenic species as reflected in the high concentrations of NO_3^-, nss $SO_4^=$, NH_4^+. Because these species (especially nss $SO_4^=$ and NH_4^+) are generally found in the radiatively-important submicron aerosol size fraction, we expect that the radiative properties of the aerosol will be largely controlled by these species. Nonetheless, mineral dust was a substantial component in most of the aerosol samples. Despite the fact that mineral dust is predominantly found in the supramicron size fraction, dust can play an important rôle in the radiative properties of the atmosphere (Li et al., 1996) and in the radiative forcing of climate (Tegen et al., 1996; Sokolik and Toon, 1996). Indeed, the aerosol in the Indian Ocean appears to be unusual in that dust and pollutants are usually mixed in relatively balanced proportions — that is, one component does not consistently dominate the other. For example, in many industrialized nations (e.g., the United States), mineral dust is a relatively minor component (Perry et al., 1998); in contrast, in areas impacted by North African aerosols, dust overwhelms all other aerosol components (Li et al., 1996). Thus, the winter monsoon Indian Ocean aerosol contains a unique mix of aerosol components that could have very unusual radiative properties. Intensive field campaigns such as those planned for INDOEX are necessary to characterize these aerosols and their radiative effects.

Although there is very little data on aerosol properties over the Indian Ocean, the data obtained during the cruise of the ORV Sagar Kanya are consistent with earlier measurements, some of which were made recently (Rhoads et al., 1998) and some in the late 1970′s (Savoie et al., 1987; Prodi et al., 1983). Thus, the transport of continental aerosol to the equatorial Indian Ocean appears to be a persistent feature that is linked with the winter monsoon. Over the longer term, we might expect aerosol concentrations in this region to increase in concert with the rapid economic development that is taking place in this region, especially on the Indian subcontinent. To more accurately assess the current radiate forcing in this region and to characterize trends, we will need long-term measurements or aerosol and radiation at the surface.

6. Acknowledgements

This paper was supported under the INDOEX program of the University of California at San Diego. The US author and co-authors thank the National Science Foundation, USA, for funding this study through the Center for Clouds, Chemistry and Climate, La Jolla, CA. This is INDOEX Publication No. 7.

REFERENCES

Ackerman, S. A. and Cox, S. K., 1982. The Saudi Arabian heat low: Aerosol distributions and thermodynamic structure. *J. Geophys. Res.* **87**, 8991–9002.

Ackerman, S. A. and Cox, S. K., 1989. Surface weather observations of atmospheric dust over the southeast summer monsoon region. *Meteorol. Atmos. Phys.* **41**, 19–34.

Angreji, P. D., 1989. Revaluation of total ozone measurements with doubloon spectrophotometer at Mt. Abu/Ahmedabad during 1951–1985. Scientific Report, ISRO-PRL-SR-34-89, Indian Space Research Organization, India, 34 pp.

Bullrich, K, 1964. Scattered radiation in the atmosphere. *Adv. Geophys.* **10**, 99–260.

Chang, C. P. and T. N. Krishnamurit, 1987. *Monsoon meteorology*. Oxford Monographs on Geology and Geophysics no. **7**.

Charlson, R. J., J. Langner, H. Rodhe, C. B. Leovy and S. G. Warren, 1991. Perturbation of the northern hemisphere radiative balance by backscattering from anthropogenic sulfate aerosols, *Tellus* **43A-B**, 152–163.

Coakley, J. A. and D. G. Baldwin, 1984: Towards the objective analysis of clouds from satellite imagery data. *J. Clim. Appl. Met.* **23**, 1065–1099.

Gairola, R. K. and T. N. Krishnamurti, 1992. Rain rates based on SSM/I, OLR and raingauge data sets. *J. Meteorol. Atmos. Phys.* **50**, 165–174.

Hameed, S. and J. Dignon, 1992. Global emissions of nitrogen and sulfur oxides in fossil fuel combustion 1970–1986. *J. Air Waste Manage. Assoc.* **42**, 159–163.

Herman, J. R., P. K. Bhartia, O. Torres, C. Hsu, C. Seftor and E. Celarier, 1997. Global distribution of UV-absorbing aerosols from Nimbus-7/TOMS data. *J. Geophys. Res.* **102**, 16911–16922.

Husar, R. B., J. M. Prospero and L. L. Stowe, 1997. Characterization of tropospheric aerosols over the oceans with the NOAA advanced very high resolution radiometer optical thickness operational product. *J. Geophys. Res.* **102**, 16889–16909.

IPCC, Climate Change, 1994. *Radiative forcing of climate change and an evaluation of the IPCC IS92 emission scenarios.* Cambridge University Press, 339 pp, ed., John T. Houghton, 1995.

Jayaraman, A., D. Lubin, S. Ramachndran, V. Ramanathan, E. Woodbridge, W. D. Collins and K. S. Zalpuri, 1998. Direct observation of aerosol radiative forcing over the tropical Indian Ocean during the Jan.-Feb. 1996 pre-INDOEX cruise. *J. Geophys. Res.* **103**, 13827–13836.

Kiehl, J. T. and B. P. Brieglab, 1993. The radiative roles of sulfate aerosols and greenhouse gases in climate forcing. *Science* **260**, 311–314.

Krishnamurti, T.N., ed. 1978. Monsoon dynamics, contributions to current research in geophysics. Birkhauser Verlag, pp. 1087–1529.

Krishnamurti, T. N., H. Pan, C. B. Chang, J. Polshay, and W. Odally, 1979. Numerical Weather Prediction for GATE. *Q. J. R. Meteor. Soc.* **105**, 979–1010.

Krishnamurti, T. N., J. Xue, H. S. Bedi, K. Ingles and D. Oosterhof, 1991. Physical initialization for numerical weather prediction over the tropics. *Tellus* **43A-B**, 53–81.

Krishnamurti, T. N., M. C. Sinha, M. Kanamitsu, D. Oosterhof, M. Fuelberg, R. Chatfield, B. J. Jacob and J. Logan, 1996. Passive forces transport-relevant to the Trace A experiment. *J. Geophys. Res.* **101**, 23, 889–907.

Li, X., H. B. Maring, D. Savoie, K. Voss and J. M. Prospero, 1996. Dominance of mineral dust in aerosol light scattering in the North Atlantic trade winds. *Nature* **380**, 416–419.

Perry, K. D., T. A. Cahill, R. A. Eldred, D. D. Dutcher and T. E. Gill, 1998. Long-range transport of Saharan dust to the eastern United States. *J. Geophys. Res.*, in press.

Prodi, F., G. Santachiara and F. Olioski, 1983. Characterization of aerosols in marine environments (Mediterranean, Red Sea, and Indian Ocean). *J. Geophys. Res.* **88**, 10957–10968.

Prospero, J. M., 1996. The atmospheric transport of particles to the ocean. In: Ittekkott, V. Honjo & Depetris, P. J. (eds.): *Particle flux in the ocean*; 1996 SCOPE, Report 57. John Wiley & Sons Ltd., 19–52.

Pszenny, A., D. Fischer, A. Mendez and M. Zetwo, 1993. Direct comparison of cellulose and quartz fiber filters for sampling submicrometer aerosols in the marine boundary layer. *Atmos. Environ.* **27A**, 281–284.

Ramanathan, V., P. J. Crutzen, J. Coakley, R. Dickerson, A. Heymsfield, J. Kiehl, D. Kley, T. N. Krishnamurti, J. Kuettner, J. Lelieveld, A. P. Mitra, J. Prospero, R. Sadourny, F. P. J. Valero and E. L. Woodbridge, 1995. *Indian ocean experiment (INDOEX) white paper, C*^{4}. Scripps Institution of Oceanography, UCSD, La Jolla, California 92093–0239, USA.

Ramanathan, V., P. J. Crutzen, J. A. Coakley, A. Clarke, W. D. Collins, R. Dickerson, D. Fahey, B. Gandrud, A. Heymsfield, J. T. Kiehl, J. Kuettner, T. N. Krishnamurti, D. Lubin, H. Maring, J. Ogren, J. Prospero, P. J. Rasch, D. Savoie, G. Shaw, A. Tuck, F. P. J. Valero, E. L. Woodbridge and G. Zhang, 1996. *Indian ocean experiment (INDOEX), a multi-agency proposal for a field experiment in the Indian Ocean, C*^{4}. Scripps Institution of Oceanography, UCSD, La Jolla, California 92093–0239, USA, 83 pp.

Rhoads, K. P., P. Kelley, R. R. Dickerson, T. P. Carsey, M. Farmer, D. L. Savoie and J. M. Prospero, 1998. The composition of the troposphere over the Indian Ocean during the monsoonal transition. *J. Geophys. Res.*, in press.

Russel, P. B. and J. M. Livingston, 1984. Slant-lidar aerosol extinction measurements and their relation to measured and calculated albedo changes. *J. Clim. Appl. Meteor.* **23**, 1204–1221.

Sarkar, S. K., H. N. Dutta, P. K. Pasricha and B. M. Reddy, 1982. *Atlas of tropospheric water vapor over the Indian subcontinent*. National Physical Laboratory, New Delhi, 164 pp.

Sasi, M. N. and Sengupta, A. 1986. *A reference atmosphere for Indian equatorial zone from surface to 80 km.* Scientific Report, SPL:SR006:85, Vikram Sarabhai Space Center, Thumbia, India.

Saunders, R. W., G. Brogniez, J. C. Buriez, R. Meerkotter and P. Wendling, 1992. A comparison of measured and modeled broadband fluxes from Aircraft data during the ICE'89 field experiments. *J. Atmos. Ocean. Technol.* **7**, 391–406.

Savoie, D. L., 1984. *Nitrate and non-sea-salt sulfate aerosols over major regions of the world oceans: concentration, sources and fluxes.* Ph.D. thesis, University of Miami. Miami, Florida, 432 pp.

Savoie, D. L., and J. M. Prospero, 1982. Particle size distribution of nitrate and sulfate in the marine atmosphere. *Geophys. Res. Lett.* **9**, 1207–1210.

Savoie, D. L., J. M. Prospero and R. T. Nees, 1987. Nitrate, non-sea-salt sulfate, and mineral aerosol over the northwestern Indian Ocean. *J. Geophys. Res.* **92**, 933–942.

Savoie, D. L., J. M. Prospero and E. S. Saltzman, 1989a. Non-seasalt sulfate and nitrate in trade wind aerosols at Barbados: Evidence for long-range transport. *J. Geophys. Res.* **94**, 5069–5080.

Savoie, D. L., J. M. Prospero and E. S. Saltzman, 1989b. Nitrate, non-seasalt sulfate and methanesulfonate over the Pacific Ocean. In *Chemical Oceanography*, vol. **10**, eds.: J. P. Riley, R. Chester and R. A. Duce. Academic, San Diego, Calif., 219–250.

Savoie, D. L., J. M. Prospero, R. Arimoto, and R. A. Duce, 1994. Non-sea-salt sulfate and methanesulfonate at American Samoa. *J. Geophys. Res.* **99**, 3587–3596.

Sokolik, I. N. and O. B. Toon, 1996. Direct radiative forcing by anthropogenic airborne mineral aerosols *Nature* **381**, 681–683.

Tegen, I., A. A. Lacis, and I. Fung, 1996. The influence of mineral aerosols from disturbed soils on the global radiation budget. *Nature* **380**, 419–422.